# Exploring the Potential of $MB_4$ (M=Cr, Mo, and W) MBenes as a High-capacity Anode Materials for Ca-ion Batteries: A DFT Approach

**M. Kashif Masood[1], Jing Wang[1,*], Juntao Song[1], Ying Liu[1,2]**

1. Department of Physics and Hebei Advanced Thin Film Laboratory, Hebei Normal University, Shijiazhuang 050024, China

2. National Key Laboratory for Materials Simulation and Design, Beijing 100083, China

* Corresponding author E-mail address: jwang@hebtu.edu.cn

## Supplementary File

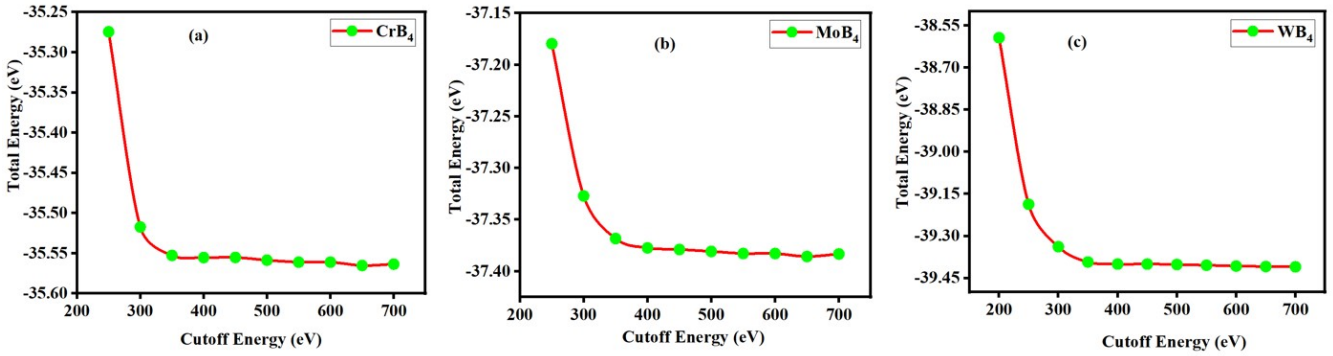


Fig.S1. Convergence test of cutoff energy for (a) $CrB_4$ (b) $MoB_4$ (c) $WB_4$

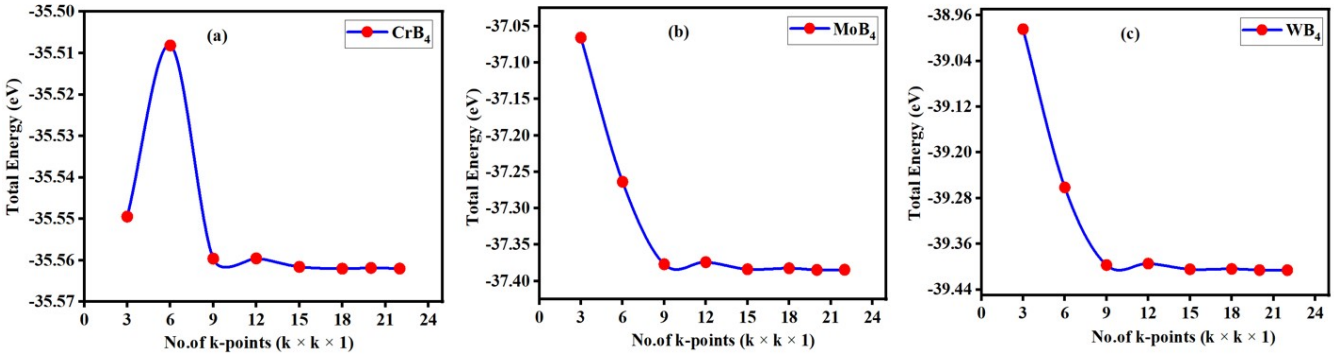


Fig.S2. Convergence test of k-points of unit cell for (a) $CrB_4$ (b) $MoB_4$ (c) $WB_4$

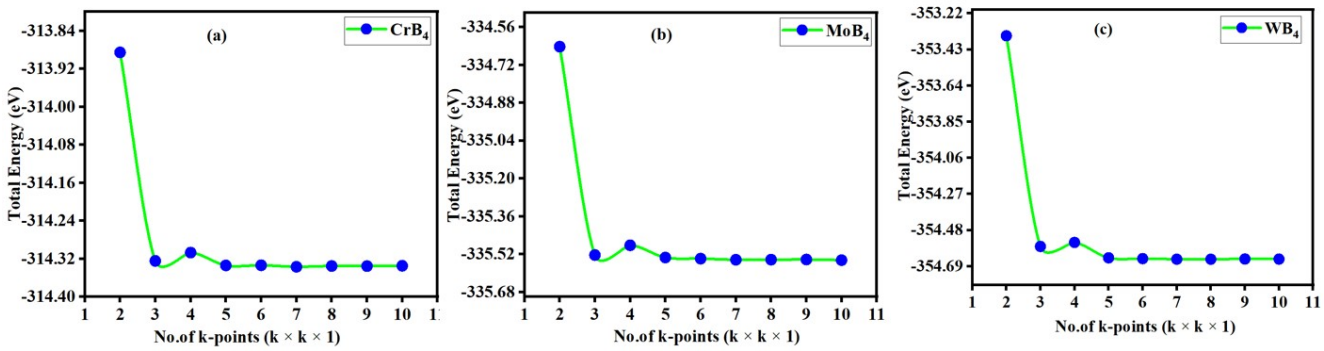


Fig.S3. Convergence test of k-points of 3×3×1 supercell for (a) $CrB_4$ (b) $MoB_4$ (c) $WB_4$

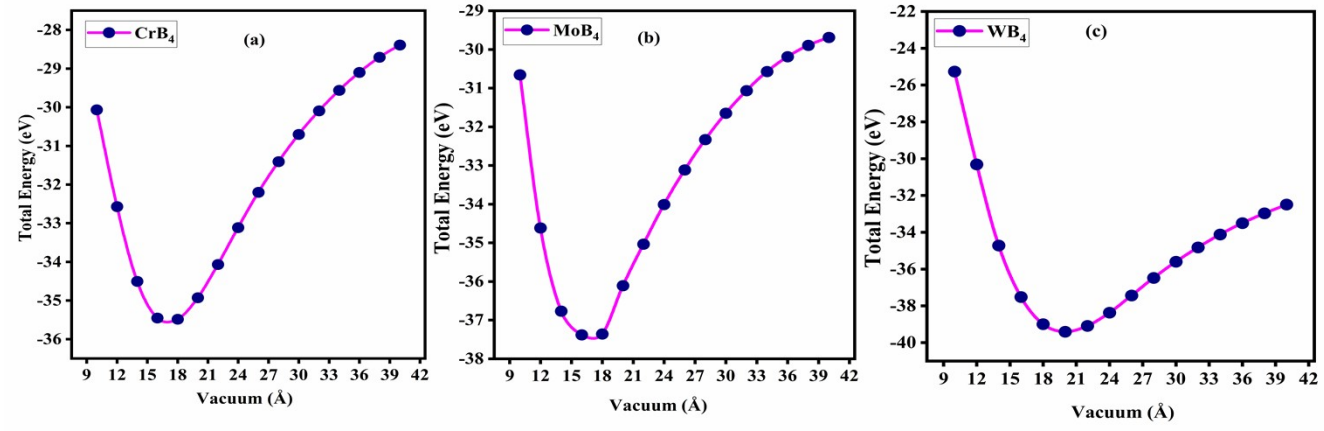


Fig.S4. Convergence test of vacuum space for (a) $CrB_4$ (b) $MoB_4$ (c) $WB_4$

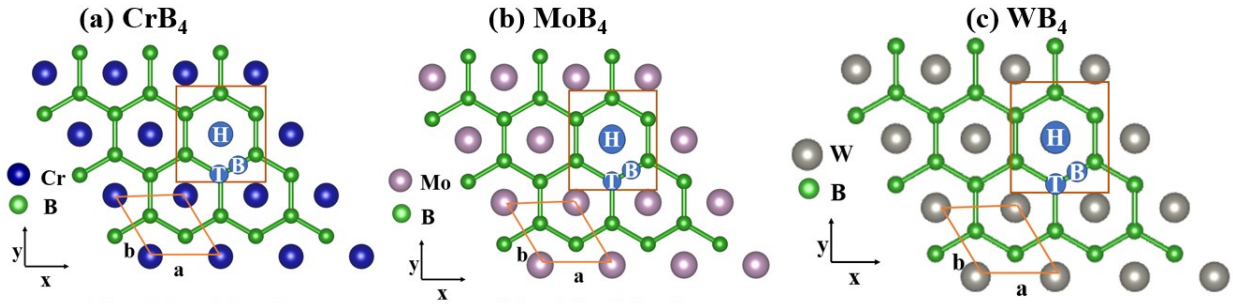


Fig.S5. Top side of Optimized structures (a) $CrB_4$ (b) $MoB_4$ (c) $WB_4$

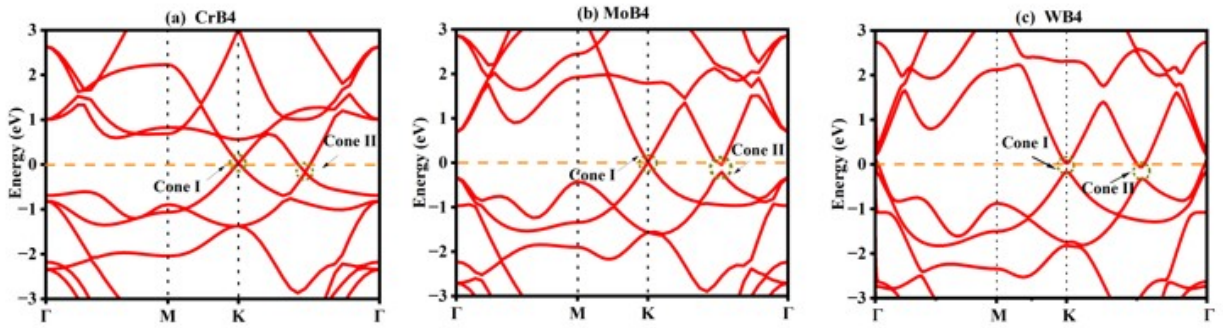


Fig.S6. Calculated 2D band structure for (a) $CrB_4$ (b) $MoB_4$ (a) $WB_4$

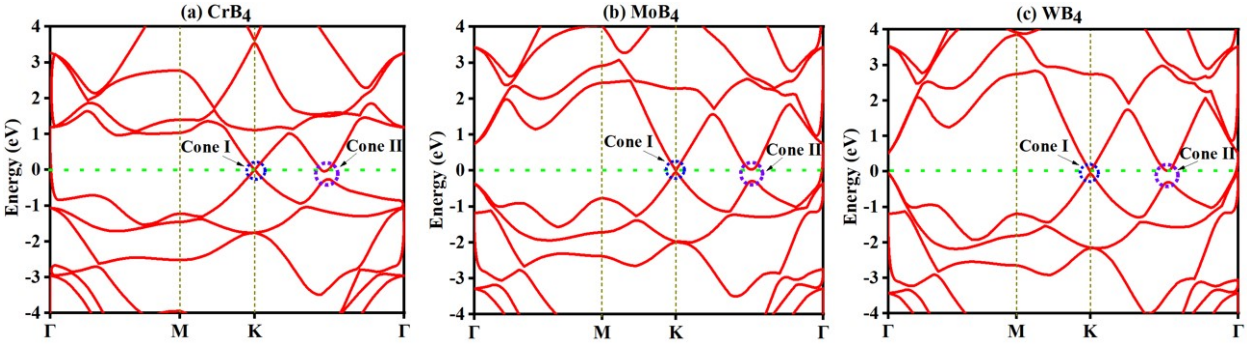


Fig.S7. Calculated 2D band structure for (a) $CrB_4$ (b) $MoB_4$ (a) $WB_4$ with HSE06 method

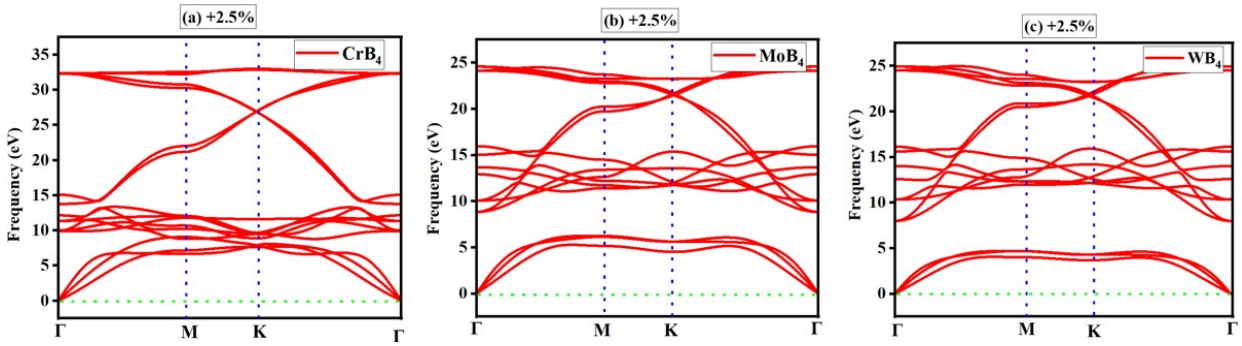


Fig. S8. Phonon dispersion curve under +2.5% strain (a) for $CrB_4$ and (b) for $MoB_4$ and (c) for $WB_4$.

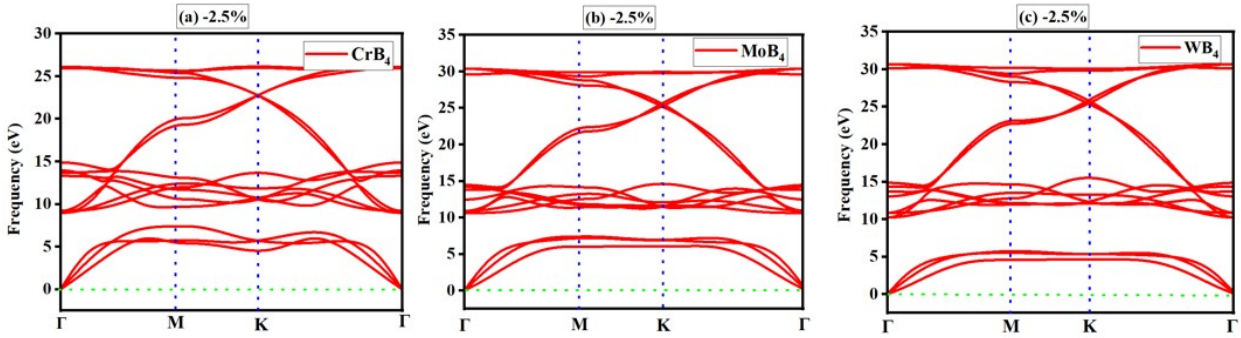


Fig. S9. Phonon dispersion curve under -2.5% strain (a) for $CrB_4$ and (b) for $MoB_4$ and (c) for $WB_4$.

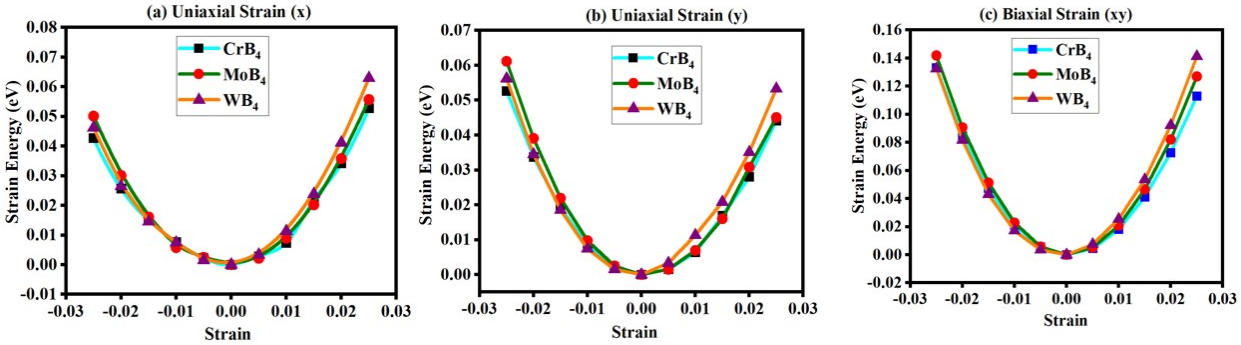


Fig.S10. The curves of strain energy for $CrB_4$, $MoB_4$ and $WB_4$ (a)with uniaxial along x-axis (b) with uniaxial along y-axis (c) with biaxial along the x- and y-axis.

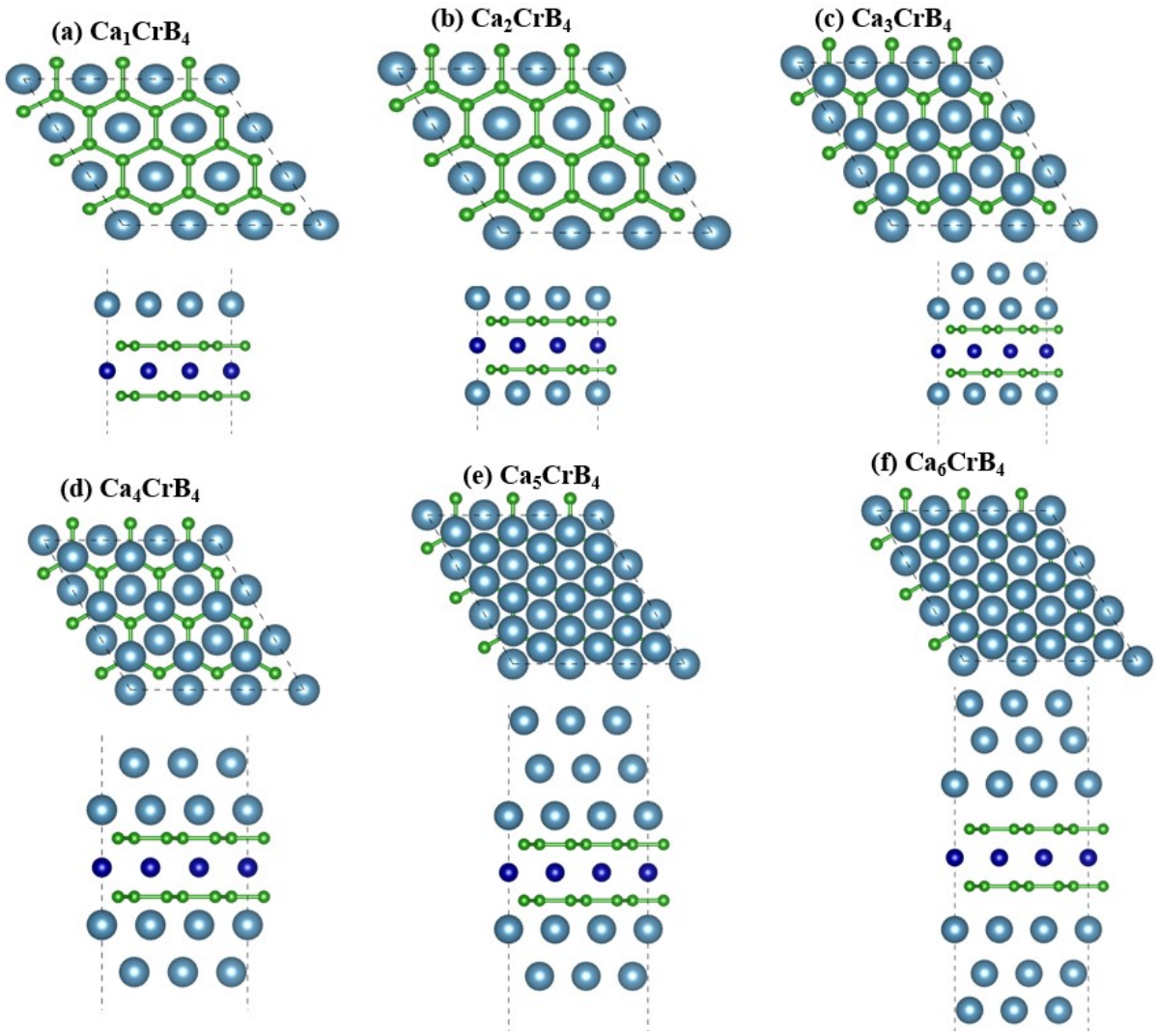


Fig. S11. (a-f) shows the top and side view of adsorption of Ca-atoms layer on $CrB_4$ from $L_1$ to $L_6$. Where each layer contains 9 Ca atoms.

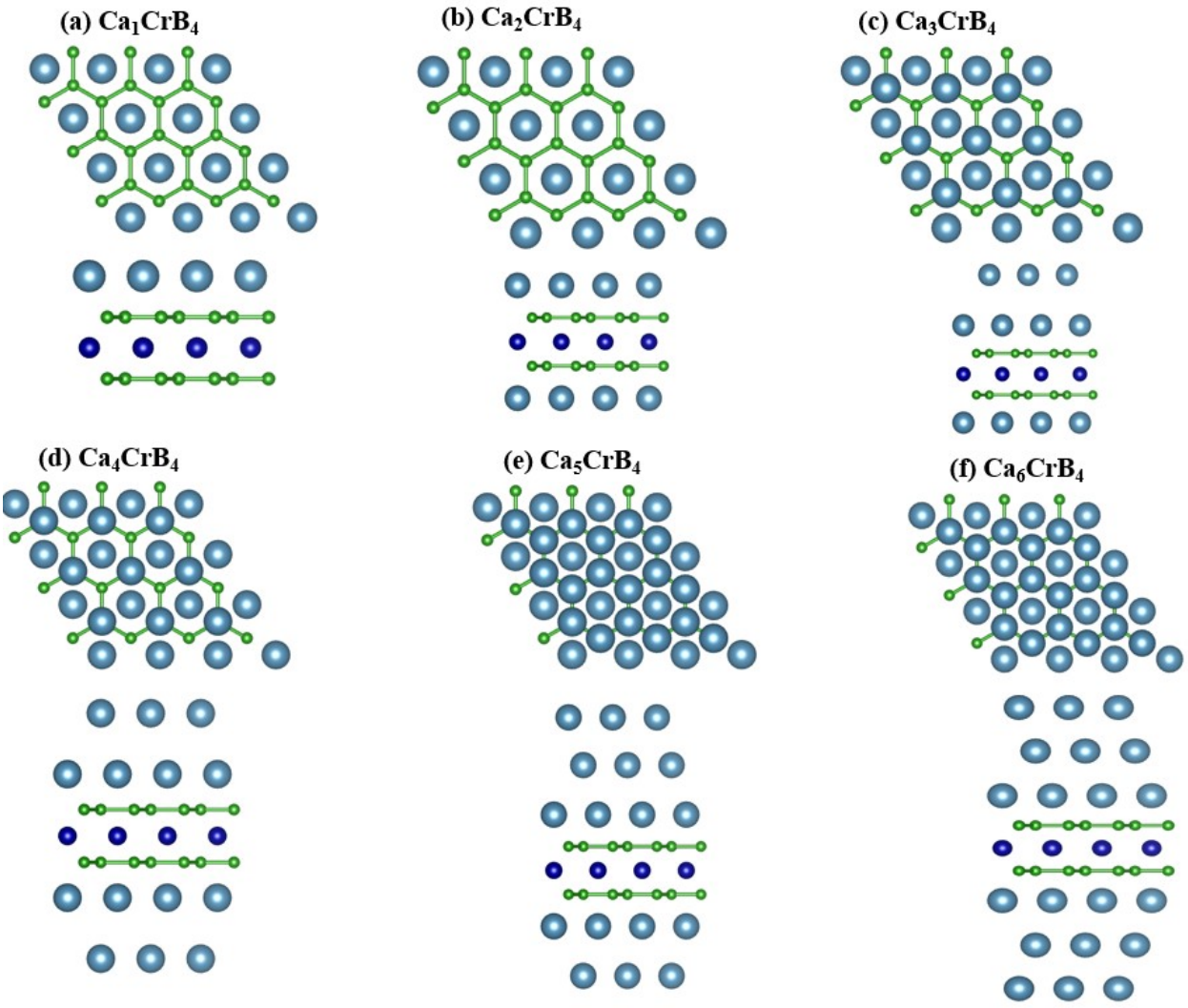


Fig. S12. (a-f) shows the top and side view of optimized structure of $Ca_xCrB_4$ (x=1,2,3,4,5,6).

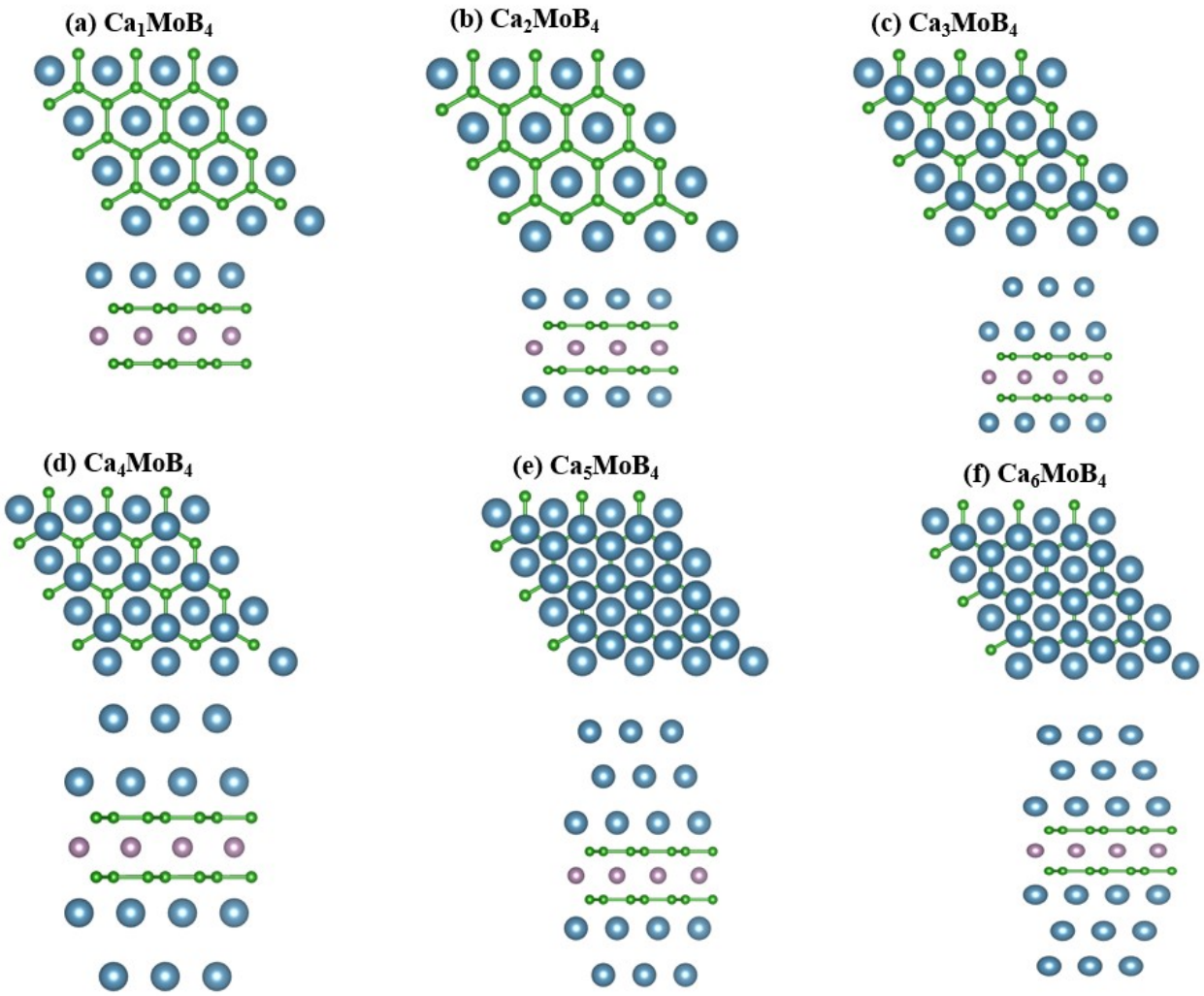


Fig. S13. (a-f) shows the top and side view of optimized structure of $Ca_xMoB_4$ (x=1,2,3,4,5,6).

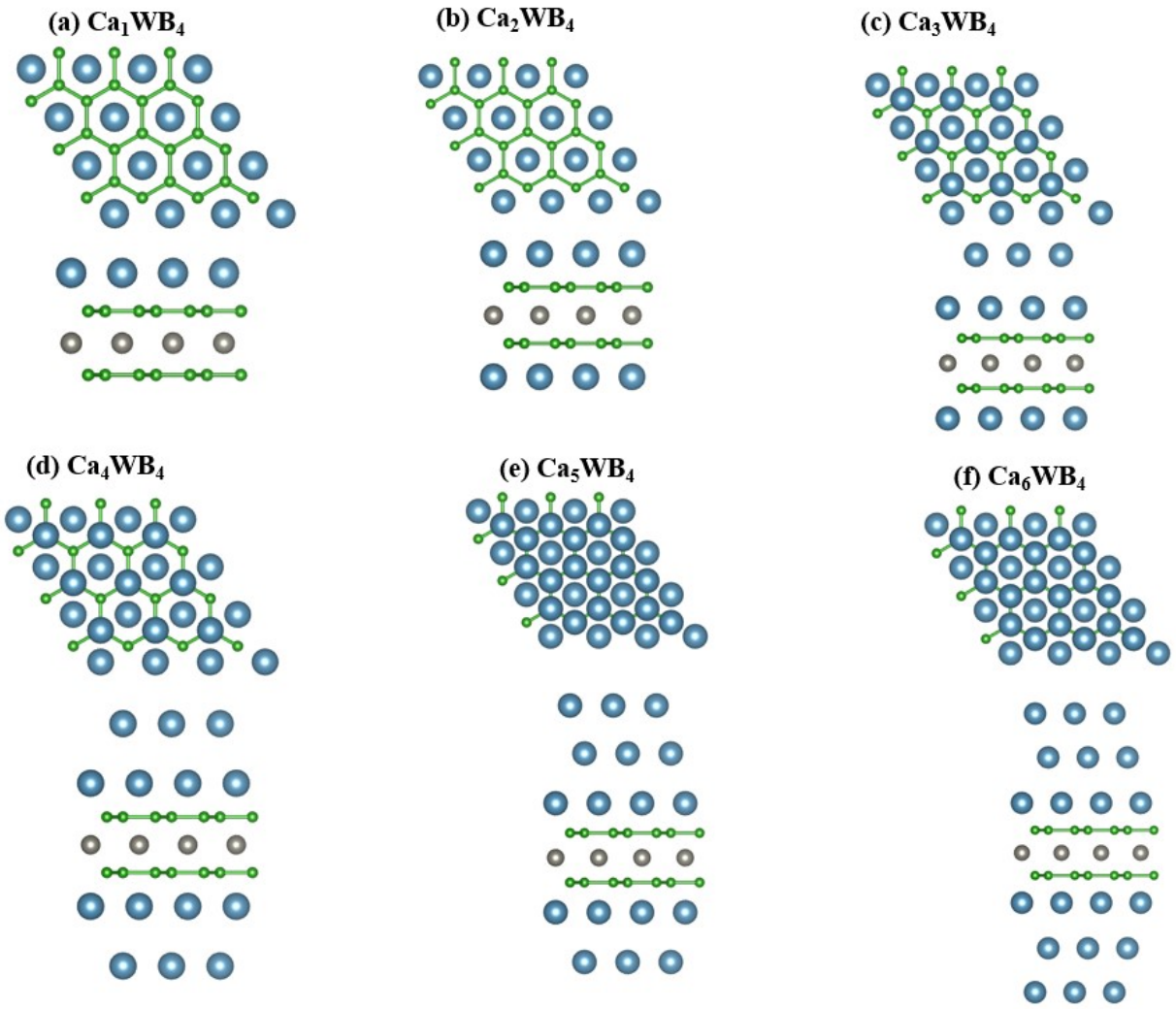


Fig. S14. (a-f) shows the top and side view of optimized structure of $Ca_xWB_4$ (x=1,2,3,4,5,6).

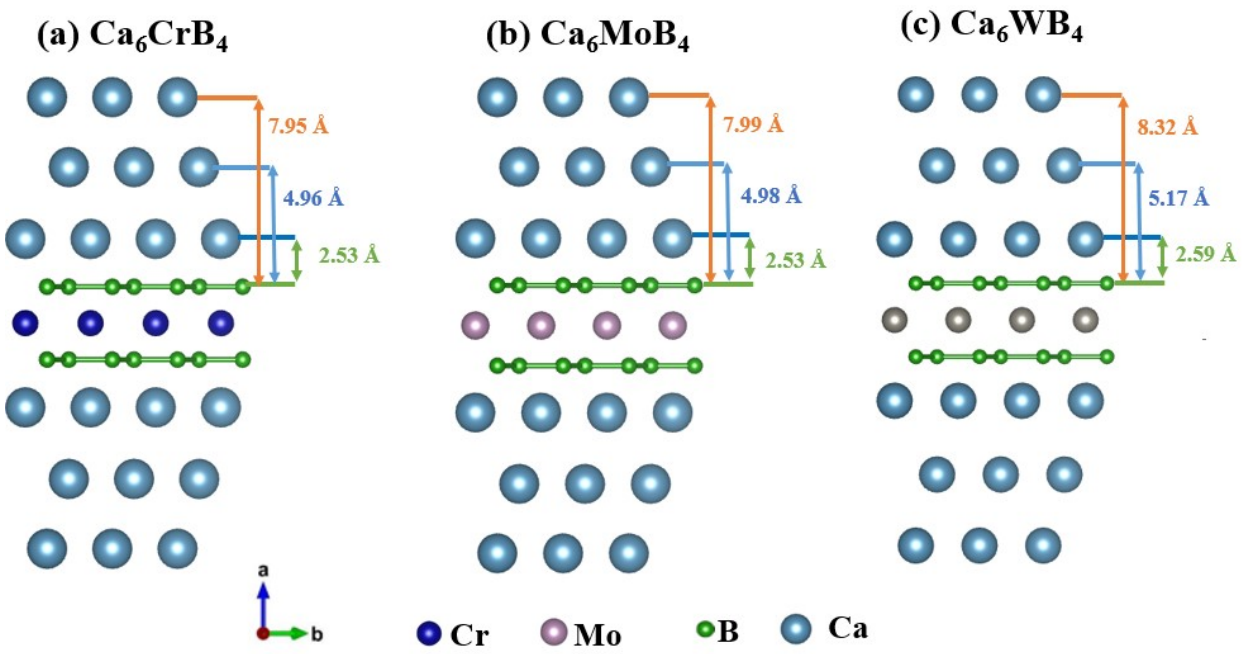


Fig. S15. Comparing the interlayer spacing between the adsorbed Ca-ions layers on the substrate (a) $Ca_6CrB_4$, (b) $Ca_6MoB_4$, and (c) $Ca_6WB_4$

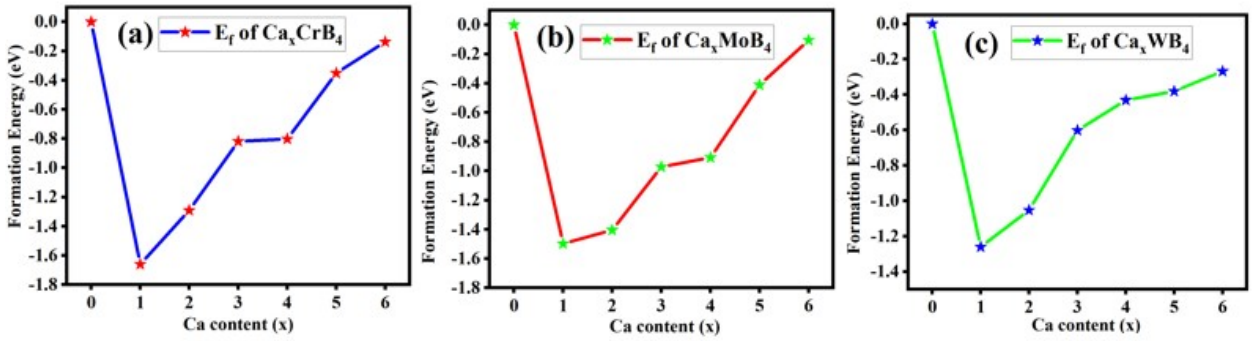


Fig.S16. Formation energy with increasing Ca content (a) $Ca_xCrB_4$, (b) $Ca_xMoB_4$, (c) $Ca_xWB_4$ at x=1,2,3,4,5,6.

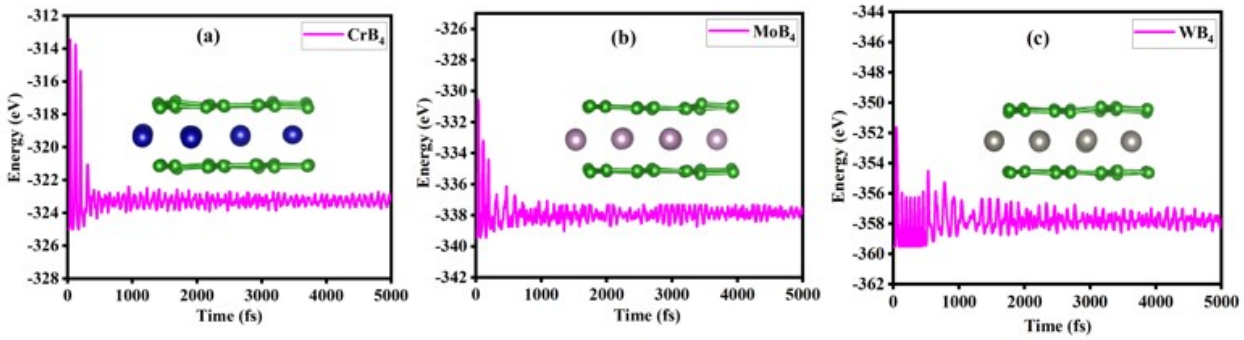


Fig. S17. Energy fluctuation vs time steps for pristine monolayer (a) $CrB_4$ (b) $MoB_4$ (c) $WB_4$

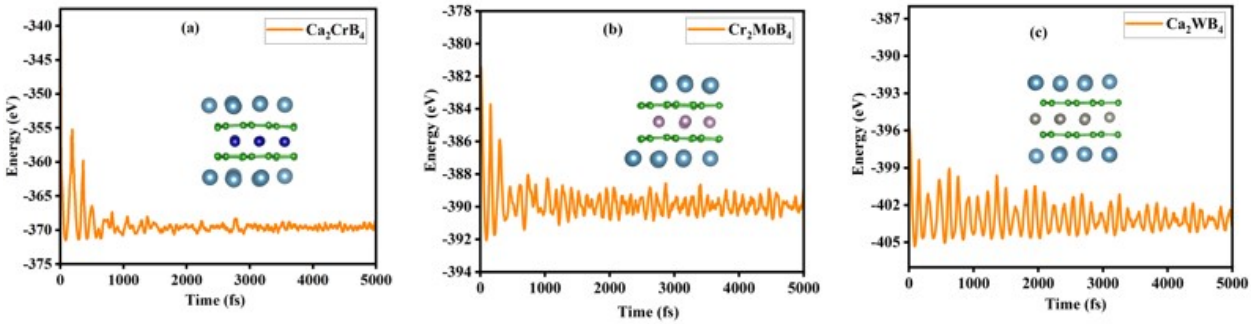


Fig. S18. Energy fluctuation vs time steps for two layer adsorbed-Ca (a) $Ca_2CrB_4$, (b) $Ca_2MoB_4$, (c) $Ca_2WB_4$

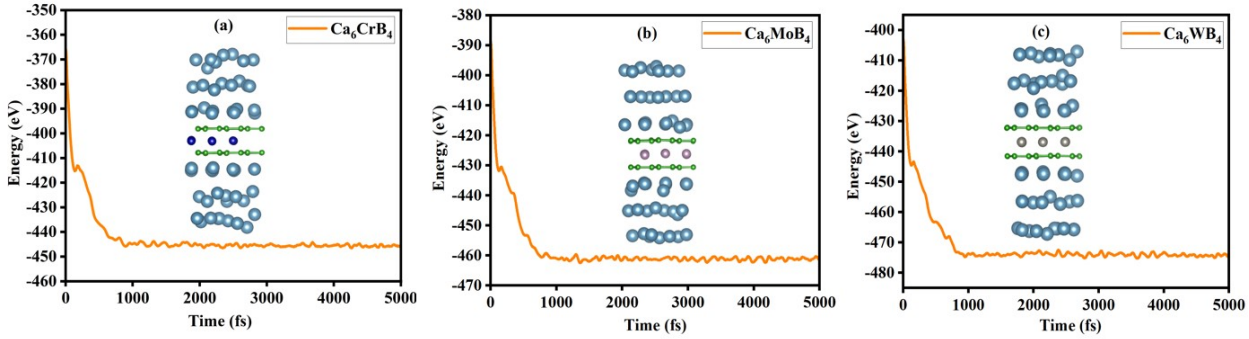


Fig. S19. Energy fluctuations vs. time duration for (a) $Ca_6CrB_4$, (b) $Ca_6MoB_4$, (c) $Ca_6WB_4$ at 300K

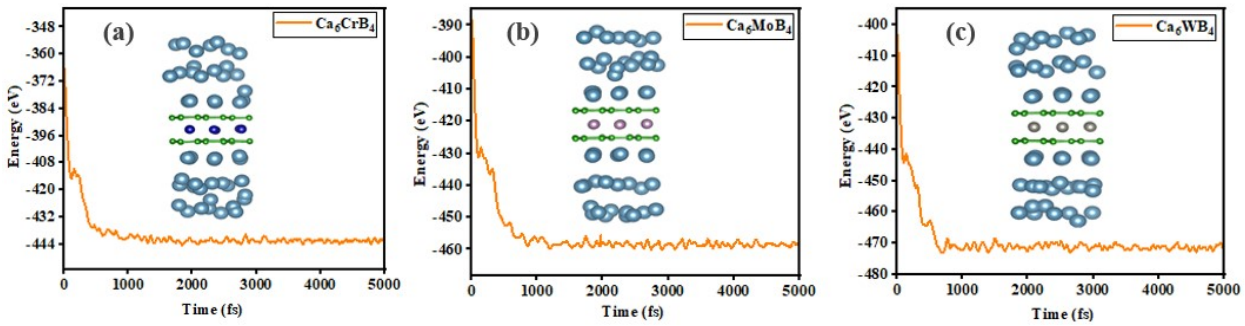


Fig. S20. Energy fluctuations vs. time duration for (a) $Ca_6CrB_4$, (b) $Ca_6MoB_4$, (c) $Ca_6WB_4$ at 500K

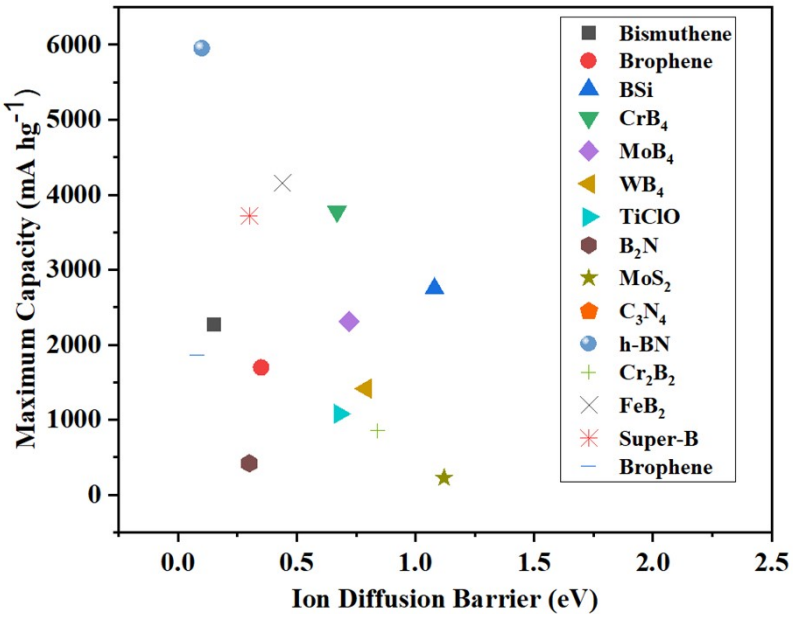


Fig. S21. Comparison of ion diffusion barrier and maximum storage capacity with the other reported anode materials.

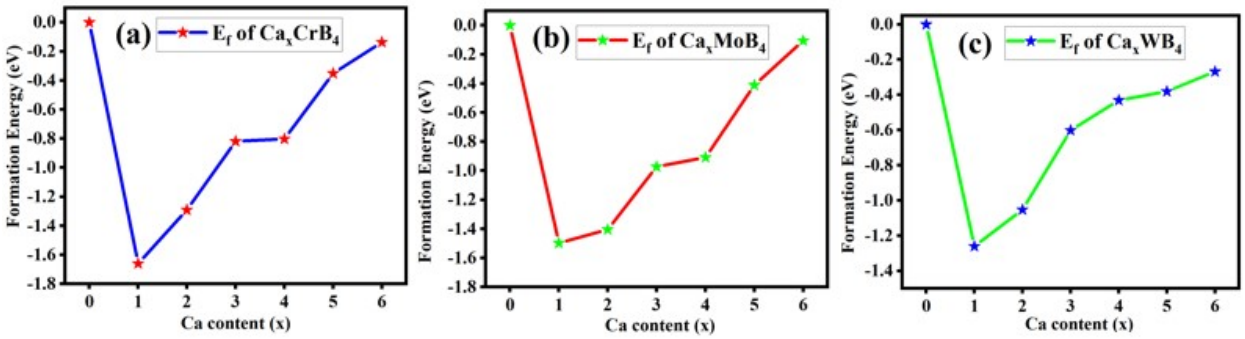


Fig. S22. Variation of lattice parameters with Ca-content (x) (a) $Ca_xCrB_4$, (b) $Ca_xMoB_4$, (c) $Ca_xWB_4$

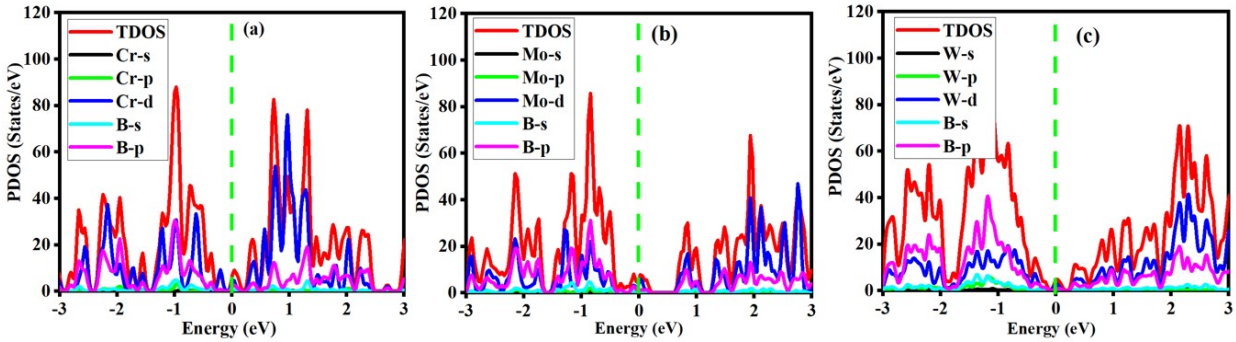


Fig. S23. PDOS with different orbitals for pristine (a) $CrB_4$ (b) $MoB_4$ (c) $WB_4$ monolayer